J. Non-Newtonian Fluid Mech. 165 (2010) 313–322

Contents lists available at ScienceDirect

Journal of Non-Newtonian Fluid Mechanics

journal homepage: www.elsevier.com/locate/jnnfm

Flow-induced polymer degradation probed by a high throughput microfluidic set-up

Philippe Nghe[a,*], Patrick Tabeling[a], Armand Ajdari[b]

[a] Microfluidique, MEMS & Nanostructures, UMR Gulliver CNRS-ESPCI 7083, Paris, France
[b] Physico-Chimie Theorique, UMR Gulliver CNRS-ESPCI 7083, Paris, France

ARTICLE INFO

Article history:
Received 9 April 2009
Received in revised form 8 October 2009
Accepted 7 January 2010

Keywords:
Semi-dilute polymer solutions
PEO degradation
Polymer scission
Microfluidics
Lab-on-a-chip
Viscosimetry

ABSTRACT

A complex fluid submitted to strong flows can endure irreversible changes in its structure. This is the case for long chain polymer additives that are commonly used as viscosity enhancers in industry, notably for oil recovery. These polymers break in solution when submitted to high deformation rates, eventually causing a serious viscosity loss. This problem of practical importance is though difficult to handle from a fundamental point of view given its complexity. We introduce here a new tool, based on microfluidic technology, for the screening of the degradation of solutions in the model situation of the flow through a constriction. We integrate two functions in a single set-up, a micro-fabricated constriction and an on-chip viscosimeter. This tool enables us to probe rapidly the viscosity loss imparted by flowing through the constriction at a given flow rate. Thanks to microfluidics, the sample preparation and measurement time are significantly lower than those implied by classical measurement protocols (reduction by up to two orders of magnitude). In addition, confinement provides control of the flow in terms of inertia. To illustrate the potential of this approach in a screening perspective, we use this tool to study the degradation of a series of semi-dilute aqueous solutions of PEO of varying molecular weights and concentrations. For each solution we identify a threshold flow rate for polymer degradation. The corresponding critical deformation rate decreases with molecular weight and concentration, as expected (the mass dependence is in line with previous reports and theories for dilute solutions). In addition we characterize the viscosity loss for larger deformation rates and find that, despite the polydispersity of our solutions, the observations for the various solutions can be roughly recast on a master curve by renormalization of the imposed deformation rates according to a law $M_w^{-1.7\pm03}c^{-0.7\pm03}$.

1. Introduction

Strong flow-induced deformations can lead to irreversible change in the structure of a complex fluid. In particular, long polymers can break in solution under strong shear or elongation. This is a significant problem in a variety of practical situations, such as turbulent drag reduction with dilute high molecular mass polymers [1] or polymer characterization methods like non-linear rheology measurements at high shear rates [2] and gel permeation chromatography (GPC). Another example of special interest to us is the use of polymers in the semi-dilute regime as viscosity enhancement additives, for example for secondary oil recovery. Here degradation due, e.g. to flow through a porous media can result in a serious loss in the efficiency of the additives.

Model experimental situations have been produced in laboratory experiments to understand how these degradation processes occur in strong extensional flow fields. In particular studies have focused on single abrupt constrictions [3–5] and cross-slot geometries, combined with birefringence and GPC measurements [6–9]. These methods give a quite detailed insight as to the resulting breakage. They are however quite time consuming (preparation, degradation in a given flow condition, measurement) to be applied to studies involving many different polymer solutions. Other studies have focused on not so well-defined geometries maybe closer to practical situations, measuring for example the global rheological properties of the fluid after passage in a porous media. It is then difficult to connect the global outcome to any microscopic event [10,11]. If a convincing picture of the onset of polymer degradation in the dilute regime in turbulent conditions has been established [12], the intrinsic complexity of the problem and that of the experiments have limited the emergence of a clear-cut understanding of the breaking mechanisms and quantification for any given flow, especially in the semi-dilute regime.

In this paper, we introduce a tool for a rough yet rapid screening the flow-induced degradation of complex fluids. We design a microfluidic device that integrates in series a well-defined degradation geometry and a viscosimeter, reducing the sample preparation

* Corresponding author at: Laboratoire Microfluidique, MEMS & Nanostructures, ESPCI, 10 rue Vauquelin, 75005 Paris, France. Tel.: +33 1 40 79 51 90.
E-mail address: philippe.nghe@gmail.com (P. Nghe).

0377-0257/$ – see front matter © 2010 Elsevier B.V. All rights reserved.
doi:10.1016/j.jnnfm.2010.01.006

volume and the measurement time by two orders of magnitude. In addition, the small scale of our flow geometry minimizes the Reynolds number, suppressing inertial instabilities which usually significantly affect polymer degradation [12]. To illustrate the potentiality of this tool, we apply it to a series of 15 PEO semi-dilute solutions, exploring their viscosity loss consecutive to a passage in a constriction as a function of the flow rate.

The layout of the remainder of this article is as follows. First, we add to this introduction a rapid review of literature results on flow-induced polymer degradation. In Section 2, we then describe our microfluidic device, its geometry and its operation. In Section 3 we present and discuss the outcome of our systematic study of PEO solutions, before closing the paper with a conclusion.

1.1. Mass dependence

A simple picture on polymer degradation is that a macromolecule of relaxation time τ in an extensional flow field with a characteristic deformation rate $\dot{\varepsilon}$ becomes quite completely stretched after a certain time if the Weissenberg number $Wi = \tau.\dot{\varepsilon} > 1$ [13,14]. In a pure extensional flow field, the stress is maximal at the centre of the chain and a force balance on the chain leads to the following relation for the force T applied to its centre:

$$T \propto \eta \dot{\varepsilon} M_w^2 \tag{1}$$

where η is the solvent viscosity, $\dot{\varepsilon}$ the elongation rate and M_w the polymer mass. At this point, the stress cumulated on the chain can lead to break a backbone bond and if one supposes that there is a critical force T_c that activates this molecular bond breakage, one obtains from relation (1) that this breakage occurs at the middle of the chain at a critical deformation rate:

$$\dot{\varepsilon}_c \propto \frac{T_c}{\eta M_w^2}. \tag{2}$$

Odell et al. [6] have refined this picture in accordance with their experiment containing a stagnation point toward agreement with the predictions of this model. Studying degradation through contractions, Nguyen and Kausch [3] have concluded that a critical deformation rate exists and scales with $M_w^{-0.95}$, attributing the discrepancy with the aforementioned result to the transient nature of their flow. Recently, a new explanation arose: taking into account the possible turbulent nature of the flow in most experiments [12], mass dependence can be re-evaluated with correct characteristic deformation rates, leading to a general agreement with the fully stretched chain breakage picture, but in a complex flow.

All these contributions lead to the conclusion that the scenario of the fully stretched chain in a pure stationary elongational flow does not generally hold and show the necessity to build experiments in which both geometry and inertia are well controlled, and ideally flow patterns can be observed.

1.2. Concentration effects

Above the entanglement concentration c^*, the interactions between chains have a dramatic effect on viscosity and viscoelastic properties. In these regimes, compared to the dilute case, a given chain feels an extra stress resulting from the hydrodynamic interactions with the surrounding other chains, thus should break more easily in the same macroscopic flow field. Experimentally, this effect has been confirmed by several groups [7,8,15], showing in all case an increase in the degradation rate with increasing concentrations. However, to date, a dependence of a critical deformation rate for degradation has not been experimentally established quantitatively for concentration effects and the theoretical ideas remain qualitative.

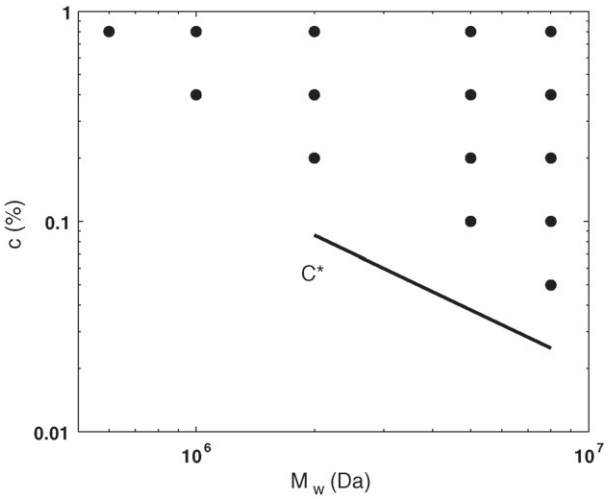

Fig. 1. Mass and concentration diagram of the aqueous PEO solutions.

2. Experimental

In this part, we first give indications about the polymer solutions we have used in this study. Then we describe the different parts of the microfluidic device: the constriction in which polymers are degraded and the viscosimeter that allows an on-line measurement of the consequent viscosity loss. We show how to bring these two parts in a same set-up. Finally, we provide experimental results to validate this measurement device.

2.1. Polymer solutions

We have chosen aqueous solutions of PolyEthyleneOxyde (PEO) as a model polymer. High average molecular weight polymers are commercially available (Sigma Aldrich) over a broad range: the average molecular weights we use span over more than one decade, from 0.6 to 8 MDa. We also vary the molecular concentration over more than one decade in the semi-dilute regime, between 0.05% and 0.8% in mass. Fig. 1 shows a map of the different mass and concentration that have been prepared with a reference line indicating c^*, estimated from zero shear viscosity measurements (Table 1) and consistently with other works on the same fluids [16,17]. These polymers are relatively polydisperse, our GPC measurements of 0.6 and 1 MDa samples indicating a polydispersity index around 1.8. We extract relaxation times λ of our solutions from the stress versus shear rate relations measured with a MCR 501 Paar rheometer in a Couette geometry, fitting them with a simple Cross model: $\eta = \eta_0/(1 + (\lambda\dot{\gamma})^n)$ with η_0 the zero shear viscosity. Zero shear viscosity η_0 and relaxation times λ are summarized in Table 1.

PEO solutions are initially prepared at concentration of 0.8% in mass. The polymer powder is homogeneously dispersed during a few seconds in a vortex of 200 mL of water created by magnetic stirring. The solution is then gently agitated on a moving table during one night to achieve dispersion of the polymer without breaking the molecules. The solution is finally homogenized by magnetic stirring during two hours at 100 rpm. Several dilutions are then prepared from this solution by adding de-ionized water and stirring again during 2 h at 100 rpm. We verify that the solutions are stable and homogeneous by measuring the viscosity of different samples. Before use, solutions are slowly driven by gravity through filters with 10 μm pores to avoid the presence of possible microgels and impurities that would block the microfluidic constriction. We check for the absence of measurable degradation at this stage, assessing the stability of their viscosity.

Table 1
Relaxation time τ and zero shear viscosity η_0 for all studied solutions of varying average molecular weights (MDa) and concentrations (wt.%). The relaxation times of the aqueous PEO solutions have been estimated with a Cross model interpretation of the stress versus shear rate relation for some solutions. For the other solutions, relaxation times indicated with a (*) have been extrapolated with the classical scaling for semi-dilute solutions $\tau \propto c^{3/2}M_w^3$, in agreement with experimental measurements on the same fluid [24].

		0.8%	0.4%	0.2%	0.1%	0.05%
8 MDa	τ (s)	3.6	1.3	0.45	*0.18	$*6 \times 10^{-2}$
	η_0 (mPa s)	7300	390	46	9.7	4.7
5 MDa	τ (s)	0.98	0.35	*0.12	$*4 \times 10^{-2}$	
	η_0 (mPa s)	2700	130	19	9.3	
2 MDa	τ (s)	43×10^{-3}	$*2 \times 10^{-3}$	$*8 \times 10^{-3}$		
	η_0 (mPa s)	67	15	3.8		
1 MDa	τ (s)	$*8 \times 10^{-3}$	$*3 \times 10^{-3}$			
	η_0 (mPa s)	20	6.1			
0.6 MDa	τ (s)	$*2 \times 10^{-3}$				
	η_0 (mPa s)	3				

Note that experiments indicate the existence of PEO chains clusters in water in quiescent dilute solutions [18], which may dissociate in strong flows [19]. The presence of these clusters is not systematic and their origin is under debate [20], but the possible interactions in view between chains (hydrogen bonding, hydrophobic interactions) are weak enough that we can assume chains individuality in our very high deformation rates flows (maintaining $\dot{\gamma} > 10^3\ s^{-1}$), even more in a regime leading to covalent bonds scission.

2.2. Microfluidic device

2.2.1. Degradation geometry

Strong extension is generally achieved by the mean of a flow through an abrupt constriction. Here we consider a 60 μm high micro-fabricated planar constriction with an abrupt entry and a progressive exit, as described in Fig. 2. The upstream zone of the constriction goes from a 500 μm wide channel to a 20 μm wide canyon-like rectangle. In Newtonian flows, this upstream zone generates a strong extensional component in the direction of the flow over a distance that is comparable to the constriction width. Inside the constriction, the solution is mainly submitted to shear and the progressive exit minimizes a second strong extensional event generated by the expansion. The characteristic elongation rate upstream the constriction equals the shear rate inside the constriction and we refer it as the nominal maximal deformation rate $\dot{\varepsilon}_d$ imposed by the geometry. Given the aspect ratio of the canyon-like constriction, we crudely evaluate $\dot{\varepsilon}_d$ by considering the Poiseuille flow of a Newtonian fluid between two parallel planes at an imposed flow rate Q. This estimate leads to the following relation:

$$\dot{\varepsilon}_d = \frac{6Q}{w^2 h} \tag{3}$$

with $h = 60\ \mu m$ the height of the constriction and $w = 20\ \mu m$ the width. In the case of viscoelastic polymer solutions, we observe corner vortices at high deformation rates upstream the constriction, in line with [17]. Given the morphology of these structures, we work under the hypothesis that that the nominal maximum imposed deformation rate $\dot{\varepsilon}_d$ remains the one imposed by the constriction. We will discuss later the influence of these structures on chain degradation.

To be able to degrade as short chains as possible, one has to go deformation rates at as high as possible. To achieve the high pressure resistance necessary, the system is molded in photocurable glue (Norland, NOA 81) from a PDMS master [21]. As indicated in Ref. [21], no deformation or leakage is observed up to 15 bars. In practice, due to pressure resistance limitations, a maximum of $\dot{\varepsilon}_d = 10^7\ s^{-1}$ can be reached for solutions which viscosity is close to the one of water.

2.2.2. The microfluidic viscosimeter

The microfluidic viscosimeter we use here is based on the idea of comparing the fluid under study with a reference fluid in a T-junction (Fig. 3). This idea has been developed and validated in other lab-on-a-chip experiments [22,23] to measure pressure differences or viscosities. The reference fluid of viscosity η_1 and a fluid of unknown viscosity η_2 are driven at equal flow rates from separated arms into a same large aspect ratio channel. Once the interface between the two fluids attains its equilibrium position, it can be shown [21] that

$$\frac{\eta_1}{\eta_2} = \frac{w_1}{w_2}, \tag{4}$$

with w_1 and w_2 the respective width occupied by the reference fluid and the studied fluid. The validity of this result has been assessed both in the case of Newtonian and complex fluids [21].

The viscosimeter is 130 μm high and is made of the same photocurable glue as the constriction. 500 nm fluorescent beads are added to the reference fluid with a typical 10^{-4} volume fraction, so that its rheology is not affected. Thanks to their size, these tracers diffuse negligibly during the measurement time and the

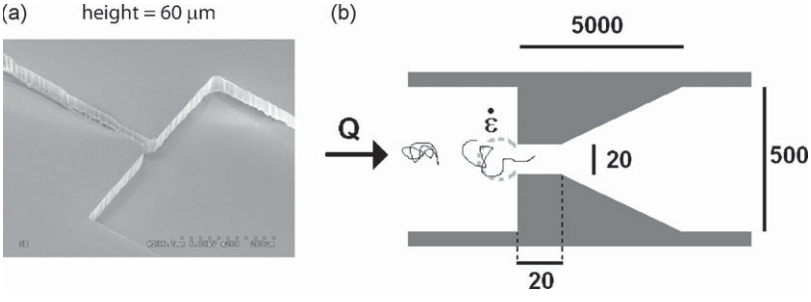

Fig. 2. (a) MEB picture of the constriction. (b) Schematic projection of the planar 60 μm high constriction. Dimensions are indicated in microns. The dotted circle line delimits the zone of strong elongation.

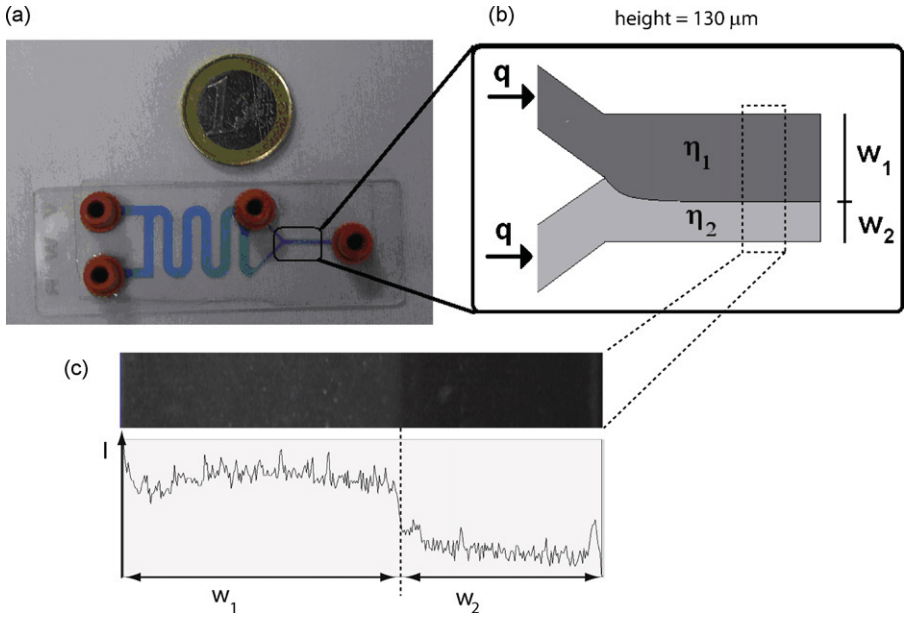

Fig. 3. (a) Picture of the chip with its connectors, the serpentine reservoir and the viscosimeter. (b) Schematic focus on the viscosimeter and its principle. (c) Experimental image of the interface and florescence intensity profile along the width from which the interface position is determined.

interface between the fluids is well defined. The sample is observed under a UV light and the position of the interface is recorded via a charged coupled device through an inverted microscope with a 10X objective.

As we want to measure the viscosity loss of a solution consecutive to polymer degradation, we use as a reference fluid the non-degraded polymer solution so that the position of the interface in the 1 mm large channel of the T-junction is directly interpreted as the viscosity ratio between the degraded and the non-degraded polymer solution. In addition, this choice of a reference fluid avoids any complication due to wetting properties and interfaces. An interesting feature of this measurement tool is that it works properly for viscosities as low as the one of water, which is of interest in our study of polymer solutions close to c^*.

2.2.3. Integration and operation of the device

We integrate the two steps described above in a same fluidic system: degradation in the constriction and measurement of the viscosity loss in the viscosimeter (Fig. 4). We mainly describe here a set-up with two separate chips, one for degradation and one for viscosity measurement, connected by tubing, but we have checked that integrating the two geometries on a same chip is possible (Fig. 5) and operates in the same way with the same performance. As we will precise more quantitatively later, due to shear-thinning of the polymer solutions, the viscosity contrast between the degraded and non-degraded solutions is better when the viscosimeter measurement shear rate $\dot{\gamma}_v$ at the wall is smaller. On the other hand, one should be able to perform polymer degradation at as high deformation rates $\dot{\varepsilon}_d$ as possible. A several order of magnitude change in the flow rate imposed by the syringe pump in a same microchannel can induce a very long transient time before reaching equilibrium, mainly due to the high hydrodynamic resistance. To avoid these relaxation phases, a valve and a reservoir are introduced between the two steps.

Operation of the lab-on-a-chip requires the commutation of the system between two modes (Fig. 4). A first mode consists in the degradation of the sample through the constriction at high flow rates and the storage of the degraded sample in the 50 μL serpentine reservoir. Turning the valve (Rheodyne 6 way) switches to a second operating mode during which the degraded sample is pushed from the reservoir into the T-junction of the viscosimeter at a low flow rate. Establishment of stable regimes in both modes requires less than 1 min. At the end, each viscosity loss measurement requires a few minutes. To study a given fluid, we fill in a 1 mL syringe and successively drive it at different flow rates. We use 100 μL of fluid per measurement, in order to rinse the tubing and fill in the reservoir for the viscosity loss measurement.

Connections (Nanoport, Up-Church) and tubing (Up-Church, 250 μm ID PEEK tubing) have been carefully chosen to be as rigid and pressure resistant as possible to minimize relaxation times. The fluid is driven through the constriction by a Harvard Apparatus syringe pump at flow rates ranging from 3 to 1600 μL/min which result in deformation rates $\dot{\varepsilon}_d$ ranging from 10^4 to $7 \times 10^6\ s^{-1}$. High precision syringe pumps (Nemesys – Cetoni) have been chosen for the viscosity measurement step to ensure temporal fluctuations lower than 1% at the flow rate of 1 μL/min, which corresponds to a viscosity measured at a deformation rate of $\dot{\gamma}_v = 5\ s^{-1}$.

2.3. Experimental validation of the device

First we test the ability to degrade polymers in the constriction separately from the microfluidic viscosimeter. We prepare 2 mL samples of PEO solutions through the constriction at different $\dot{\varepsilon}_d$ and measure their resulting viscosity in a commercial rheometer (Contraves Low-shear 30). Fig. 6a shows the non-linear rheology of a 0.4% 5 MDa PEO solution before and after different degradation conditions $\dot{\varepsilon}_d$, showing a decreasing viscosity with increasing $\dot{\varepsilon}_d$, which corresponds to a higher degradation rate at higher deformation rates. Making the ratio between the initial viscosity and the degraded one, we obtain the viscosity loss for each $\dot{\varepsilon}_d$ measured at different shear rates $\dot{\gamma}_m$ in the rheometer (Fig. 6b). This ratio has a plateau value for $\dot{\gamma}_m$ below approximately the inverse of relaxation time of the native solution, and increases for higher $\dot{\gamma}_m$ as an effect of shear-thinning. As a consequence already mentioned in

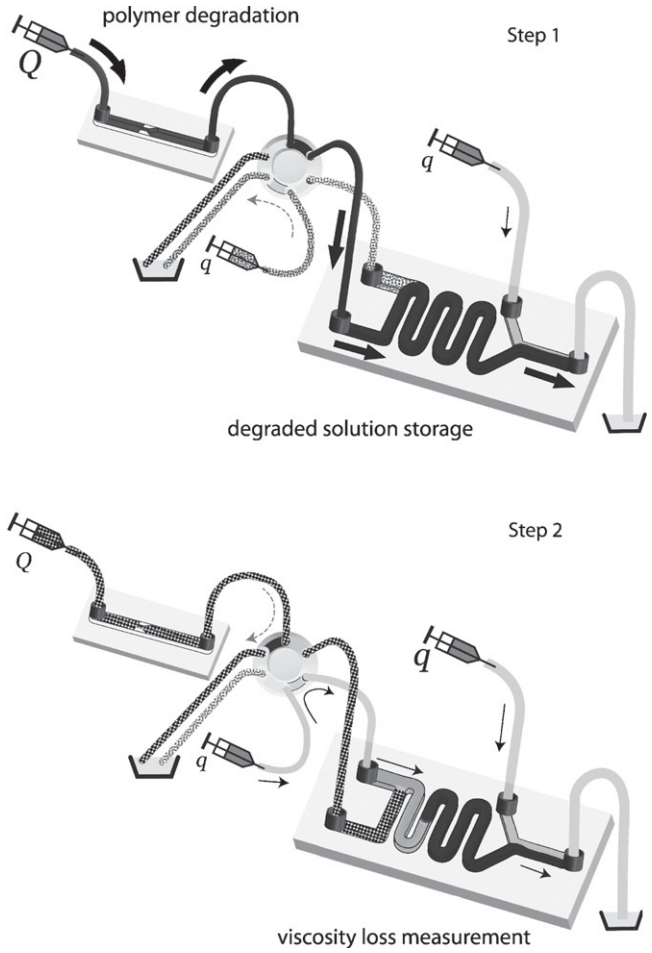

Fig. 4. Integration and operation of the microfluidic set-up. All the syringes contain the same native non-degraded polymer solution, which has been seeded with fluorescent tracers in the case of the two syringes driven at the low flow rate Q. Shade off colours indicate parts that are not useful during the corresponding step and in which residual fluid is or steady or relaxes to trash (the two basin). During step 1, polymer solution is pushed at a high flow rate Q through the constriction chip and is then driven through the valve to the serpentine reservoir; to ensure that the fluid pushed from the reservoir goes to trash, non-degraded polymer solution is driven in parallel at Q in the other arm of the T-junction to trash. During step 2, polymer solution is pushed at a low flow rate Q through the valve and enters the serpentine reservoir to push the solution of degraded polymers formerly prepared during step 1; as a result, in the T-junction, degraded and non-degraded polymer solutions are pushed side by side at a same flow rate Q to perform the viscosity loss measurement.

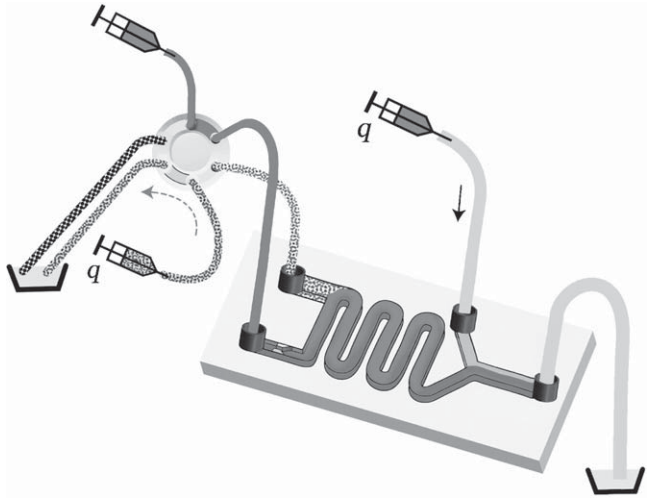

Fig. 5. Design equivalent to the one of Fig. 4 on a unique chip.

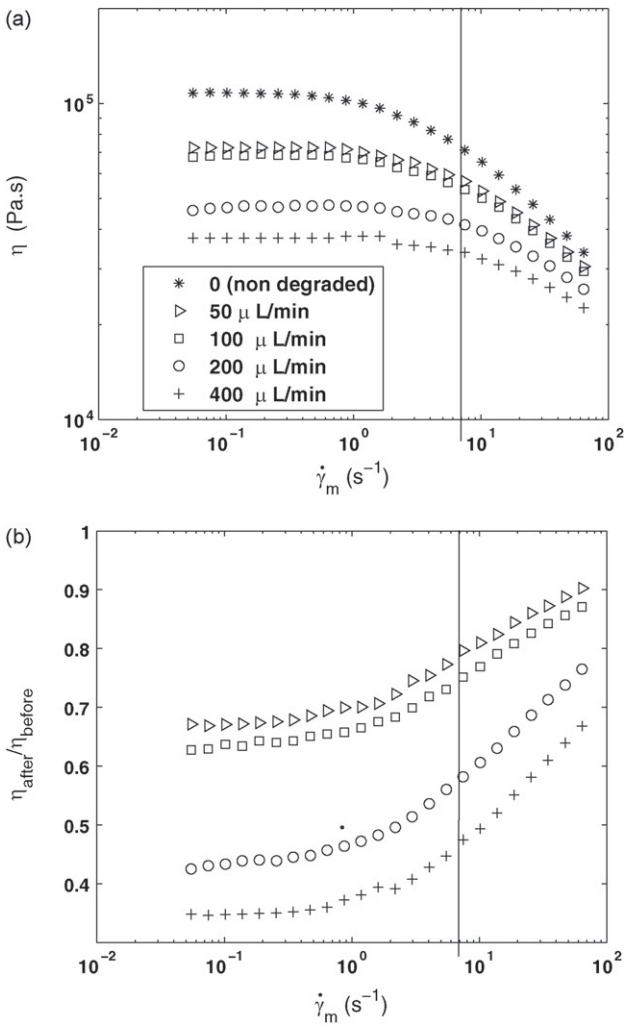

Fig. 6. (a) Viscosity curves measured in a Low-shear 30 rheometer of non-degraded and degraded 0.4% 5 MDa PEO solutions prepared in the constriction at different flow rates (in μL/min): 0 (*), 50 (triangles), 100 (squares), 200 (o), 400 (+). The vertical line indicates the shear rate at which viscosity ratio is measured inside the microfluidic viscosimeter. (b) Ratio between the viscosity before and after degradation.

Section 2.2.3, the measurement of the degradation by the viscosity loss in the chip should be made at as low-shear rates as possible for a better viscosity contrast.

In a second step we verify that the viscosity measured in the microfluidic viscosimeter agrees with the value obtained in a commercial rheometer, both in the Newtonian and non-Newtonian case. Glycerol and water mixtures with known viscosities ranging from 1.05×10^{-3} to 1.3×10^{-3} Pa s are measured in the viscosimeter with water as a reference fluid (Fig. 7). Besides, different PEO aqueous solutions are degraded in the constriction at different values of $\dot{\varepsilon}_d$. Given a degradation condition $\dot{\varepsilon}_d$, we measure in the commercial rheometer the consecutive viscosity $\eta_{rheo}(\dot{\gamma}_m)$, where $\dot{\gamma}_m$ is the measurement shear rate, and compare it to a value $\eta_{chip}(\dot{\gamma}_v) = \eta_{native} \times r$, where η_{native} is the viscosity of the non-degraded solution measured in the commercial rheometer and r the viscosity ratio between the degraded and non-degraded solution measured in the viscosimeter with a shear rate at the wall chosen equal to $\dot{\gamma}_m$. Using three different PEO solutions and varying $\dot{\varepsilon}_d$ and $\dot{\gamma}_m$, we can see in Fig. 7 that the values obtained in the commercial rheometer and the microfluidic chip agree over a wide range of viscosities.

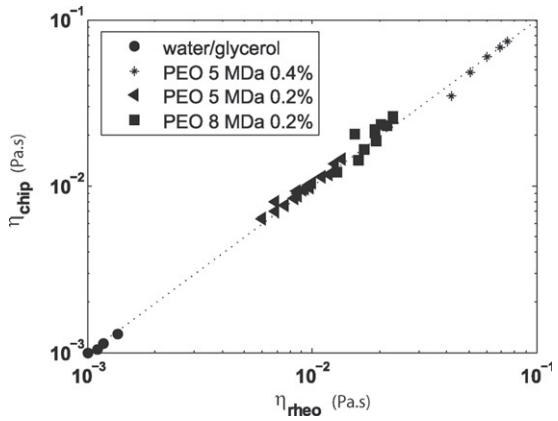

Fig. 7. Comparison between the viscosity measured in a Low-shear 30 rheometer and measured in the chip for water and glycerol mixtures and 3 different PEO solutions degraded at different flow rates. For each point, the measurement shear rate in the Couette rheometer $\dot{\gamma}_v$ equals the measurement shear rate at the wall of the chip viscosimeter $\dot{\gamma}_m$. For the polymer solutions, measurement shear rates have been varied between 5.5 and 63.9 s^{-1}.

3. Results and discussion

3.1. Flow break-up of PEO solutions

We perform degradation experiments in the microsystem for PEO solutions of average molecular weights and concentrations indicated in Fig. 1. More than a decade is covered for each parameter, the polymer mass ranging from 0.6 to 8 MDa and the concentration from 2 to 16 times c^* for the 8 MDa PEO solution. Varying the flow rate through the constriction in the degradation mode (as explained in Section 2.2.3), we measure the consecutive viscosity ratio between the degraded and non-degraded solution for different values of $\dot{\varepsilon}_d$, nominal maximum deformation rate imposed in the degradation geometry. The viscosity ratio after degradation is represented for a particular PEO solution in Fig. 8. Given the operating time described in Section 2.2.3, obtaining such a curve requires around 2 h with the microfluidic set-up instead of the several days of sample preparation for a commercial rheometer. We also show the results for other PEO solutions representative of the whole dynamical range of the experiment (Fig. 9). On this last plot, we average the viscosity ratio for each

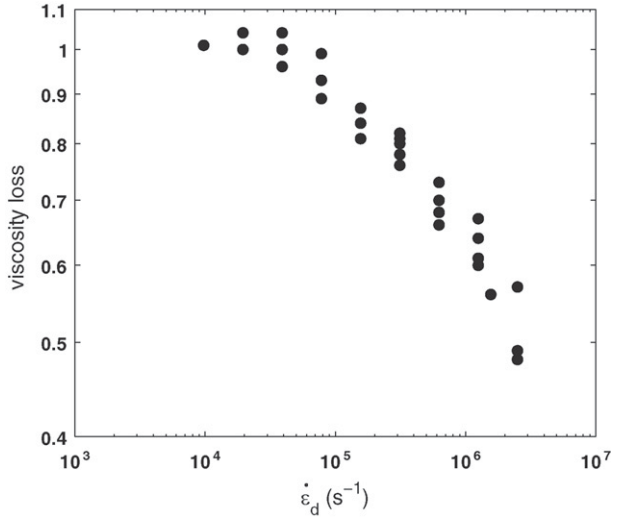

Fig. 8. Viscosity ratio measured in the chip at $\dot{\gamma}_m = 5.5$ s^{-1} versus the maximum imposed deformation rate $\dot{\varepsilon}_d$ for a 0.4% 5 MDa PEO solution.

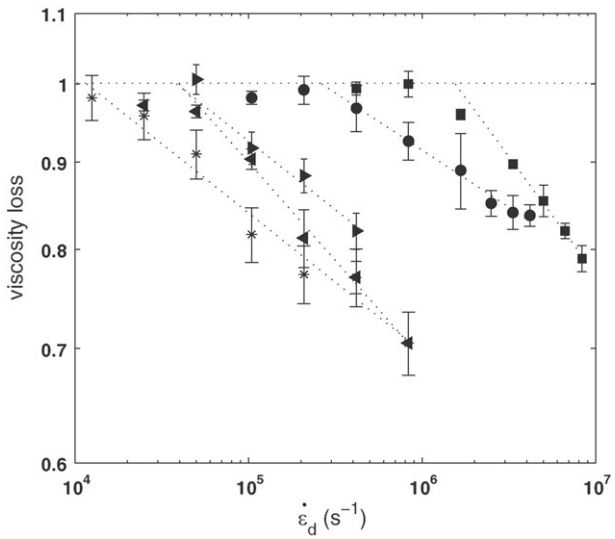

Fig. 9. Viscosity loss of 0.8% PEO solutions of varying mass: 8, 5, 2, 1 and 0.6 MDa with the linear fit of the points representing a significant viscosity loss. For clarity reasons, only the solutions corresponding to the five top points in Fig. 1 have been represented.

$\dot{\varepsilon}_d$ over 4 measurements and obtain the error from the standard deviation.

In a logarithmic representation, the viscosity ratio consists in a plateau region around the value 1 (no degradation) followed by a significant decay after a certain value of $\dot{\varepsilon}_d$. The typical error on the viscosity ratio measurement is 5%. As a consequence, we consider that the decay of the viscosity ratio is significant for a value below 0.95 and we forget the data points above this threshold to perform the analysis of the viscosity ratio decay. We also do not consider values below 0.6 to ensure uniformity of the data analysed over the samples. Then we fit the viscosity ratio decay by a power law and obtain from it two parameters. The intersection of the fit with the viscosity ratio value of 1 determines a critical value $\dot{\varepsilon}_c$ for the beginning of significant degradation of the polymers.

3.2. Analysis of the mass and concentration dependence

As explained above, viscosity loss becomes significant above a certain deformation rate $\dot{\varepsilon}_c$. This critical deformation rate for degra-

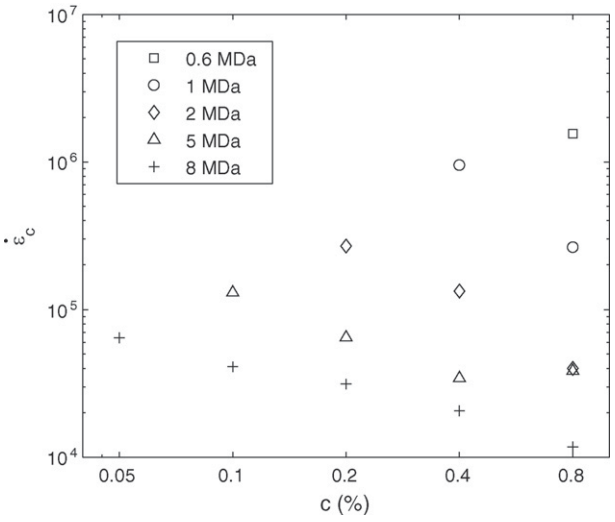

Fig. 10. Critical deformation rate $\dot{\varepsilon}_c$ for degradation versus concentration for different polymer average molecular weights.

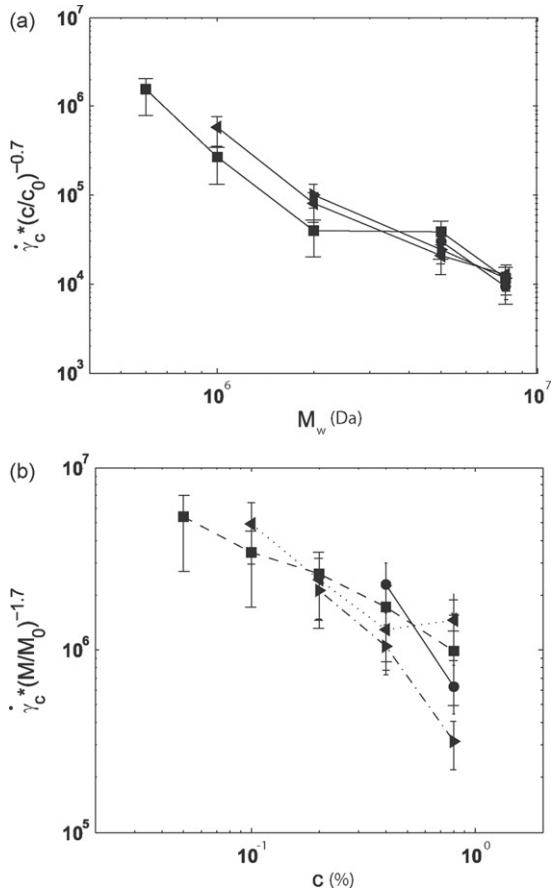

Fig. 11. (a) Mass dependence of the critical deformation rate $\dot{\varepsilon}_c$ rescaled by its concentration power law dependence. (b) Concentration dependence of the critical deformation rate $\dot{\varepsilon}_c$ rescaled by its mass power law dependence.

dation $\dot{\varepsilon}_c$ decreases with polymer mass and concentration (Fig. 10). To quantify this trend in terms of scaling laws, we fit the surface given by these points by a plane on a logarithmic representation for mass, concentration and critical deformation rate. We get from the fit two exponents: one for the mass dependence and one for the concentration dependence. It comes that $\dot{\varepsilon}_c$ varies like $M_w^{-1.7\pm03}$ and $c^{-0.7\pm03}$. To give a better idea of these dependences, we plot in Fig. 11a the projection of the mass dependence of $\dot{\varepsilon}_c$ rescaled by $c^{-0.7}$ and in Fig. 11b the projection of the concentration dependence of $\dot{\varepsilon}_c$ rescaled by $M_w^{-1.7}$.

Now, we can use these exponents to rescale all the viscosity ratio curves by the mass and concentration power law dependence. The 0.8% 0.6 MDa PEO solution is taken as a reference for c_0 and M_0 and we renormalize $\dot{\varepsilon}_d$ by $(M_w/M_0)^{-1.7}\,(c/c_0)^{-0.7}$. All the curves roughly reassemble on a master curve (Fig. 12). This curve confirms that the power law fitting is appropriate to describe the decay with a uniform exponent over approximately one decade above the critical deformation rate $\dot{\varepsilon}_c$.

3.3. Comment on the influence of shear-thinning on the viscosity loss measurement

We have used $\dot{\gamma}_v = 5.5\,s^{-1}$ as the lowest feasible measurement shear rate in our on-chip viscosimeter, but the 5 and 8 MDa polymer solutions are already shear-thinning in this deformation rate domain (Fig. 6a with a vertical line at $\dot{\gamma}_v = 5.5\,s^{-1}$). We evaluate here how far viscosity loss measurement performed in a shear-thinning regime can change the value of $\dot{\varepsilon}_c$. Note yet that two identical non-degraded solutions always have a viscosity ratio

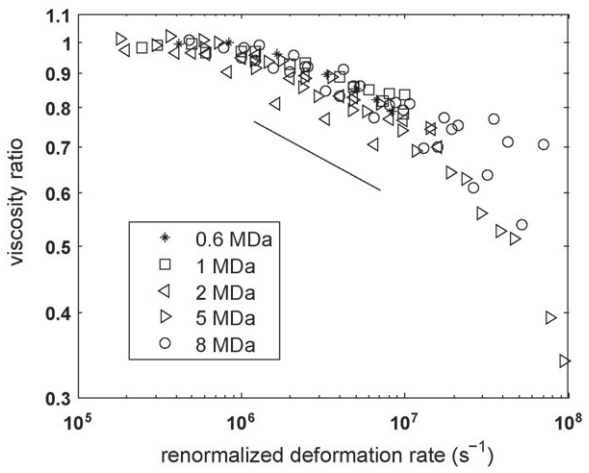

Fig. 12. Viscosity loss curves versus a renormalized imposed deformation rate $\dot{\varepsilon}_d \times (M_w/M_0)^{1.7}(c/c_0)^{0.7}$. This collapse is obtained for all the solutions prepared with the characteristics represented in Fig. 1. For a given mass, the different concentrations are represented by a same symbol. The straight line indicates the mean slope obtained from the viscosity decay fit as represented on the few solutions of Fig. 8.

equal to 1 whatever the measurement shear rate $\dot{\gamma}$, so that an analysis of the beginning of viscosity decay should not be strongly dependent on the shear-thinning effect.

To evaluate the contribution of shear-thinning, we consider the data of viscosity loss obtained in Section 2.3 for PEO 5 MDa 0.4% solutions (Fig. 6b). In this case, for each degradation condition, viscosity loss has been measured at different measurement shear rates in a Couette rheometer. At each given measurement shear rate, we plot the viscosity loss versus imposed deformation rate for degradation and apply a power law fit to interpret the viscosity loss decay, similarly to what we have done for all solutions in Section 2.3. This fit indicates a critical deformation rate for degradation $\dot{\varepsilon}_c$. Due to shear-thinning, we observe a dependence of $\dot{\varepsilon}_c$ on the measurement shear rate in the rheometer $\dot{\gamma}_m$: $\dot{\varepsilon}_c$ tends to be over-estimated (Fig. 13) in the shear-thinning regime. We include this contribution in the lower error bar in the data of Fig. 11. This solution is one of the worst cases in terms of shear-thinning and the consequent contribution to the error is similar to initial dispersion of the experimental values, so that final results of Section 3.2 are not modified.

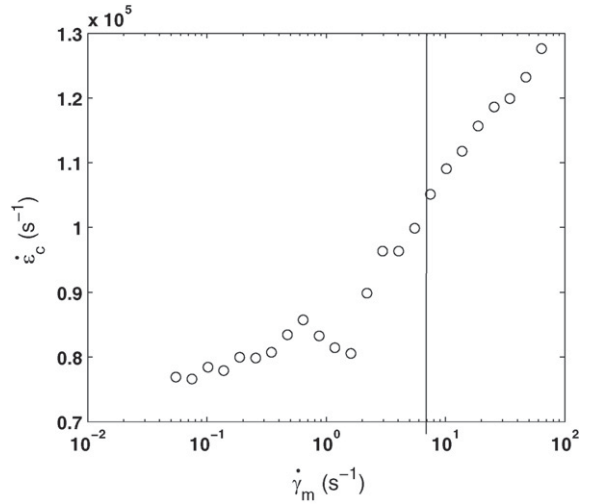

Fig. 13. Critical deformation rate for the onset of polymer degradation extrapolated at different measurement shear rates $\dot{\gamma}_m$ for the data of Fig. 6.

3.4. Discussion

Thanks to our integrated microfluidic device, we have been able to get a broad set of data on polymer degradation over a range of very different average molecular weights and concentrations, observing trends in qualitative agreement with the simplest descriptions of the phenomena. Beyond these qualitative trends, and despite the significant polydispersity of our samples ($M_w/M_n = 1.8$), our quantitative measurements outcome can be roughly rationalized using scaling laws in terms of mass and concentration, which we now comment upon.

Experimental [3,6–9] and numerical studies [24,25] of the critical deformation rate for breaking for monodisperse dilute solutions report a $\dot{\varepsilon}_c \propto M_w^{-\alpha}$ dependence, with $1 \leq \alpha \leq 2$. The exponent $\alpha = 1.7 \pm 0.3$ we find for our polydisperse semi-dilute solutions is in the range of these previous results. On the fundamental side, given that breakage rate is higher for high molecular weight chains and that the viscosity we measure depends on molecular weight distribution, direct quantitative interpretation of our viscosity loss curves in terms of a microscopic scenario of chain scission seems difficult to reach. On a practical side, as applications often involve solutions of polydispersity comparable to that of our samples, our result may have a use as an estimate.

If we try now to understand the history of a chain in our geometry, we have to notice that the simple scenario of complete chain stretching followed by scission described in the Section 1.1 relies on trapping a chain an indefinite time in a pure and constant elongation flow field. Actually, direct visualization of DNA under flow [14] has demonstrated the importance of the residence time to achieve full unfolding. As a consequence, in transient flows, in addition to the polymer relaxation time and the deformation rate, one has to take into account the strain cumulated on the chain. The strong dependence of this strain on the geometry has led to interpret in a first time the exponent $\alpha \approx 1$ found in constriction experiments [3] as the result of chain breakage before full stretching in transient flows, according to the "yo-yo" model which describes chain unravelling as a centro-symmetric process [26].

In our abrupt contraction, based on simple hydrodynamic considerations for Newtonian flows, characteristic times for the imposed deformation and the residence in the extensional zone both equal the inverse of the shear rate inside the constriction (circa $\dot{\varepsilon}_d^{-1}$). Two consequences are that the residence time in the upstream zone is decreased while Weissenberg number is increased and the shear contribution of the inner part of the constriction is comparable to the one of the extension zone. As a whole, predicting the resulting state of a chain is not obvious. In addition the discussion of residence time is further complicated by an effect emphasized in semi-dilute solutions (as alluded to in Section 2.2.1): because of their viscoelasticity, vortices appear upstream of the contraction (as discussed in Refs. [17,27]). As can be confirmed by visual observation of solutions with fluorescent tracers, these vortices grow with the imposed Weissenberg number and become unstationary. The resulting growth of the strong extension region zone before the constriction likely impacts the cumulated strain on the chain and could promote unfolding. Considering these elements and our value of α closer to 2 than to 1, we cannot exclude full unfolding of the chain in our transient geometry, on the opposite to partial unfolding discussed in Ref. [3]. To be conclusive, it would be very interesting if future studies could measure how unfolding of a chain is affected by the effective geometry created in viscoelastic constriction flows without inertial perturbations, in particular in the case of the high Weissenberg numbers at the onset of degradation, which range in our experiment between 10^3 and several 10^4.

Importantly, discussion about the transient nature of the flow as an explanation for the different scalings has been recently challenged by the experiments of Islam et al. [9] and Vanapalli et al. [12], who point out the role of inertia. Both apparent $\dot{\varepsilon}_c \propto M_w^{-2}$ and M_w^{-1} dependences are found in a same stagnation point geometry, based on the Reynolds number Re being, respectively, below or above 1000 [9]. Going further, the authors of [12] show that most of the literature experiments have been performed in turbulent conditions, and that all the corresponding data can be interpreted with a unified picture, considering the viscous drag on an extended chain in such a complex flow. In this interpretation framework, the deformation rates imposed at high Re are re-computed in all literature experiments, showing that a M_w^{-2} law holds generally (neglecting a logarithmic dependence) both in turbulent and laminar conditions, whatever the geometry. This consideration is directly related to our miniaturized geometry that achieves to date the only example of polymer degradation in transient flows without inertial perturbations. Actually, we mainly keep the condition $Re < 100$ for all flows, below the onset $Re_c = 370$ for the onset of inertial instabilities in contraction-expansion geometries indicated in Ref. [12], the absence of inertial instabilities being confirmed by direct observation of the flow patterns allowed by the transparent microfluidic device. Hence, our value of α significantly different from 1 and consistent with 2 supports the possibility of complete chain unfolding in transient flows. Given the universality of the interpretation of Vanapalli et al. [12] in the case of dilute solutions, we comment more quantitatively possible links between our results and this work in Appendix.

Our last point is about the influence of concentration on polymer degradation (a point on which very few experimental reports exist and essentially no theoretical prediction). Conceptually, one can go back to the single-chain picture used for dilute solutions, and argue that the effect of the surrounding semi-dilute medium may be roughly described by an effective viscosity (larger than that of the solvent as included in Eq. (1)). Unfortunately, introducing an effective shear or extensional viscosity to model the chain environment is not obvious because of the very high deformation rates. Practically, in terms of concentration dependence, our experiment confirms the trend found by all the other studies [7,8,15] and shows that the concentration dependence of the deformation rate threshold lies between $c^{-0.4}$ and c^{-1}. We leave here quantitative understanding of the concentration dependence and its interplay with mass dependence as an opened issue.

4. Conclusion

Two aims have been achieved in this work: the design of a new tool useful for screening the degradation of polymers in solution and the study of mass and concentration dependence of this degradation.

Thanks to microfluidic technology, we have been able to reduce by two orders of magnitude the necessary volume for a viscosity measurement. Consequently the sample preparation time is reduced by the same factor from hours to minutes. This enables us to explore and reproduce different degradation conditions over a large dynamical range and with a few mL of fluid. This last feature is especially interesting for testing new polymer formulations produced in minute quantities. Thanks to a specific fabrication technology, high pressures can be reached in a micron-sized constriction. The microfluidic context leads to very high deformation rate while keeping the control of flow in terms of inertia, allowing direct observation at the same time. To integrate the degradation and the viscosity measurement on a same set-up, decoupling these two steps with a valve and reservoir system is shown to be necessary, mainly because of the very different flow conditions needed in these two steps. We have mainly described a set-up made of two separate chips, but integration on a same chip is equivalent (Fig. 5).

We have applied this tool to a set of polydisperse PEO solutions over a wide range of size and concentration. To our knowledge, this is a first systematic study of the variation of the degradation rate with concentration and mass in the semi-dilute regime, which is in practice of great importance for applications using polymers as viscosity enhancer. We find a critical deformation rate for the onset of polymer degradation that decreases with the average molecular weight and concentration (in line with other studies). This critical deformation rate scales roughly as $M_w^{-1.7\pm0.3}c^{-0.7\pm0.3}$ and this scaling allows us to collapse the "viscosity loss versus imposed deformation rate" curves for the various PEO solutions on a master curve. Although direct microscopic interpretation of this scaling is difficult given the polydispersity of our samples ($M_w/M_n \approx 1.8$), such a representation may yet provide a useful guide for semi-dilute solutions of practical use.

The mass scaling we find in our constriction geometry is significantly different from the ones obtained in past experiments of transient flows of dilute monodisperse polymer solutions. A possible explanation for this discrepancy is that degradation occurs in turbulent conditions in former experiments [12] and in a flow free from inertial instabilities in our. However in our case, viscoelasticity of the solutions induces complex flow patterns upstream the constriction which role should be quantified, but which may be of very different nature than inertial turbulence.

Perspectives for this work are (as our results) twofold. On an instrumentation side, this microfluidic tool or variants could be applied to the study of the flow-induced degradation of other type of complex fluids, as a practical way to screen with a decent throughput their resistance to severe conditions met for examples in extensional flows, in turbulent flows, or when flown through porous media. As to the understanding of the degradation of polymer solutions, a direction would be to repeat such studies with monodisperse solutions of different chemistry, while at the same time quantifying the flow patterns induced by the viscoelasticity of these solutions and their effect on chain unfolding.

Acknowledgements

The authors acknowledge Total for funding this research. They acknowledge Michel Cloitre, Ilias Iliopoulos, Guylaine Ducouret, Clémentine Locatelli and Anne-Claire Dumanois for their precious help.

Appendix A.

As we have mentioned in Section 3.4, the work of Vanapalli et al. [12] gives a general picture of the onset of polymer degradation in dilute solutions, assessing the turbulent character of the flows which have been explored to date. Our work explores a range of Reynolds numbers several decades lower than the data used in Ref. [12] for contraction-expansion geometries and comparison to this synthesis of most of the results of literature can be instructive. Using similar backbone bond strength of 2.3 nN for PEO, we plot in Fig. 14 data from our most diluted solutions along with the predictions for dilute PEO solutions shown in Fig. 4B of Ref. [12]. The lowest concentration for each average molecular weight we have tested corresponds to a weakly entangled state around $2c^*$.

We see here that our apparent critical Re numbers (or equivalently our critical deformation rates for significant viscosity loss) exceed the prediction for laminar flow within one decade. This result, in addition to the overestimation of Re (shown as a horizontal error bar in Fig. 14), indicates that onset of degradation may occur at deformations rates lower than those needed for significant viscosity loss. This is encouraging for pursuing this type of study, either with a more sensitive characterization device in the dilute case, or by imposing stronger or repeated degradation events before viscosity measurement in the semi-dilute case, and eventually characterizing the onset of degradation in laminar flows.

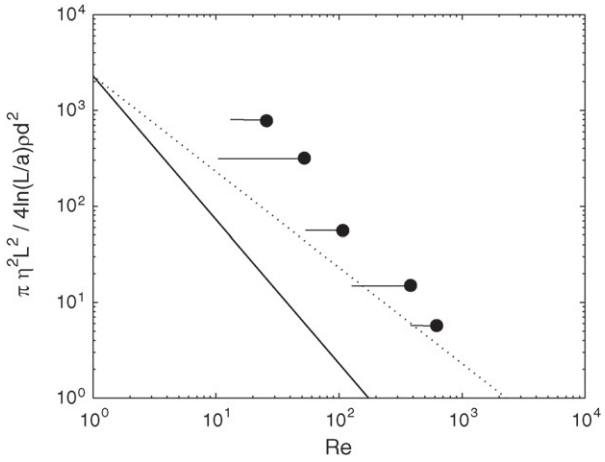

Fig. 14. Critical Reynolds number for significant viscosity loss compared to the predictions of the onset of dilute PEO degradation in Fig. 4B of Ref. [12], for the turbulent case (full line) and laminar case (dotted line). We compare here our most diluted solutions of average molecular weights of 8, 5, 2, 1 and 0.6 MDa with respective concentrations of 1.8, 2.4, 2.3, 2.6 and $3.5c^*$. Re is estimated with the solvent viscosity, but effective viscosity of these lowly entangled solutions at high deformation rates may be higher, as indicated by the horizontal error bar.

References

[1] R.W. Paterson, F.H. Abernath, Turbulent flow drag reduction and degradation with dilute polymer solutions, J. Fluid Mech. 43 (1970) 689.
[2] K. Kang, L.J. Lee, K.W. Koelling, High shear microfluidics and its application to rheological measurement, Exp. Fluids 38 (2005) 222.
[3] T.Q. Nguyen, H.H. Kausch, Chain scission in transient extensional flow kinetics and molecular weight dependence, J. Non-Newtonian Fluid Mech. 30 (1988) 125.
[4] T.Q. Nguyen, H.H. Kausch, Effects of solvent viscosity on polystyrene degradation in transient elongational flow, Macromolecules 23 (1990) 5137.
[5] J.D. Clay, K.W. Koelling, Molecular degradation of concentrated polystyrene solutions in a fast transient extensional flow, Polym. Eng. Sci. 37 (1997) 5.
[6] J.A. Odell, A. Keller, Y. Rabin, Flow-induced scission of isolated macromolecules, J. Chem. Phys. 88 (1988) 4022.
[7] J.A. Odell, A.J. Muller, K.A. Narh, A. Keller, Degradation of polymer solutions in extensional flows, Macromolecules 23 (1990) 3092.
[8] A.J. Muller, J.A. Odell, S. Carrington, Degradation of semidilute polymer solutions in elongational flows, Polymer 33 (1992) 12.
[9] M.T. Islam, S.A. Vanapalli, M.J. Solomon, Inertial effects on polymer chain scission in planar elongational cross-slot flow, Macromolecules 37 (2004) 1023.
[10] C. Noïk, P. Delaplace, G. Muller, Physico-chemical characteristics of polacrylamide solutions after mechanical degradation through a porous medium, Soc. Petrol. Eng. 28954 (1995).
[11] J.A. Odell, S.J. Haward, Viscosity enhancement in non-Newtonian flow of dilute aqueous polymer solutions through crystallographic and random porous media, Rheol. Acta 25 (2006) 853.
[12] S.A. Vanapalli, S.L. Ceccio, M.J. Solomon, Universal scaling for polymer chain scission in turbulence, PNAS 103 (2006) 16660.
[13] P.G. de Gennes, Coil-stretch transition of dilute flexible polymers under ultrahigh velocity gradients, J. Chem. Phys. 60 (1974) 5030.
[14] T.T. Perkins, D.E. Smith, S. Chu, Single polymer dynamics in an elongational flow, Science 27 (1997) 2016.
[15] B.A. Buchholz, J.M. Zahn, M. Kenward, G.W. Slater, A.E. Barron, Flow-induced chain scission as a physical route to narrowly distributed, high molar mass polymers, Polymer 45 (2004) 1223.
[16] V Tirtaatmadja, G.H. McKinley, J.J. Cooper-White, Drop formation and break-up of low viscosity elastic fluids: effects of molecular weight and concentration, Phys. Fluids 18 (2006) 043101.
[17] L.E. Rodd, T.P. Scott, D.V. Boger, J.J. Cooper-White, G.H. McKinley, The inertio-elastic planar entry flow of low-viscosity elastic fluids in micro-fabricated geometries, J. Non-Newtonian Fluid Mech. 129 (2005).
[18] D.L. Ho, B. Hammouda, S.R. Kline, Clustering of poly(ethylene oxide) in water revisited, J. Polym. Sci., Part B: Polym. Phys. 41 (2003) 135.
[19] A.M. Shetty, M.J. Solomon, Aggregation in dilute solutions of high molar mass poly(ethylene) oxide and its effect on polymer turbulent drag reduction, Polymer 50 (2009) 261.

[20] K. Devanand, L.G. Leal, Polyethylene oxide does not necessarily aggregate in water, Nature 343 (1990) 739.
[21] D. Bartolo, G. Degre, P. Nghe, V. Studer, Microfluidic stickers, Lab Chip 8 (2008) 274.
[22] A. Groisman, S.R. Quake, A microfluidic rectifier: anisotropic flow resistance at low Reynolds number, Phys. Rev. Lett. 92 (2004) 094501.
[23] P. Guillot, P. Panizza, J.B. Salmon, M. Joanicot, A. Colin, Viscosimeter on a microfluidic chip, Langmuir 22 (2006) 6438.
[24] K.D. Knudsen, J.G. Hernandez Cifre, J. Garcia de la Torre, Conformation and fracture of polystyrene chains in extensional flow studied by numerical simulations, Macromolecules 29 (1996) 3603.
[25] C.C. Hsieh, S.J. Park, R.G. Larson, Brownian dynamics modelling of flow-induced birefringence and chain scission in dilute polymer solutions in a planar cross-slot flow, Macromolecules 38 (2005) 1456.
[26] G. Ryskin, Calculation of the effect of polymer additive in a converging flow, J. Fluid Mech. 178 (1987) 423.
[27] 1L.E. Rodd, J.J. Cooper-White, D.V. Boger, G.H. McKinley, Role of the elasticity number in the entry flow of dilute polymer solutions in micro-fabricated contraction geometries, J. Non-Newtonian Fluid Mech. 143 (2007) 170.